AIMS Mathematics, 11(5): 12934–12960.
DOI: 10.3934/math.2026532
Received: 20 January 2026
Revised: 15 April 2026
Accepted: 28 April 2026
Published: 11 May 2026

https://www.aimspress.com/journal/Math

Research article

l_1-embeddability of pentagon-based open-ended nanotubes and its applications

Guangfu Wang*, **Chunxiao Xu and Wenchao Cong**

School of Mathematics and Information Sciences, Yantai University, Yantai 264005, China

* **Correspondence:** Email: gfwang@ytu.edu.cn.

Abstract: A graph is l_1-embeddable if it admits a binary addressing such that the Hamming distance between the binary addresses is, up to scale, the distance in the graph between the corresponding vertices. The zigzag pentagon-based nanotubes and armchair pentagon-based nanotubes are two new materials with the tube shapes. In order to easily calculate their chemical indices based on distances, we showed that only five types $\mathcal{I}(p,1)$, $\mathcal{I}(1,q,\theta)$ with $q \geq 5$, $I(1,3,\theta)$, $I(2,3,\zeta)$ and $I(2,5,\zeta)$ zigzag pentagon-based nanotubes were l_1-embeddable. Finally, we gave the precise value of the Wiener index and the hyper-Wiener index of these five zigzag pentagon-based nanotubes.

Keywords: l_1-graph; zigzag pentagon-based nanotubes; armchair pentagon-based nanotubes; the Wiener index
Mathematics Subject Classification: 05C09, 05C12, 05C92

1. Introduction

Zhang et al. [1] discovered a novel steady-state carbon allotrope composed exclusively of carbon pentagons. Additionally, they found that regardless of chirality, when curled, pentagon-based nanotubes can be formed, which possess semiconducting properties. It can be inferred from the article by Zhong and Chen [2] that a novel metastable three-dimensional carbon allotrope, entirely composed of pentagonal rings, has been identified. Structures composed entirely of pentagons have garnered significant attention across various research fields, including but not limited to [3, 4].

As mentioned in [5], the idea of embedding graphs into a "nice" metric space with low distortion is being applied more widely in the design and analysis of algorithms. A "nice" metric space means that its structural properties have been extensively studied, such as Euclidean space and l_1-space. In approximation algorithms for graph and network problems, applications such as shortest cut [6] and minimum bandwidth [7] make the study of low-distortion embeddings itself an important topic.

Therefore, the study of metric spaces is often regarded as a way to study the structure of a given

metric space: If an embedding of metric space M_1 into widely studied metric space M_2 can be found, then the intrinsic structural theorems in M_2 can be used.

For a graph G, let $V(G)$ and $E(G)$ be its vertex set and edge set, respectively. The *distance* $d_G(u, v)$ between two vertices u and v of G is the length of a shortest path connecting u and v. If the graph G is clear from the context, then we simply write $d(u, v)$.

Let X be a set. A function d: $X\times X \to \mathbb{R}^+$ is called a *metric* on X if d satisfies that (*i*) $d(x, y) = d(y, x)$; (*ii*) $d(x, y) = 0$ if and only if $x = y$; and (*iii*) $d(x, z) \leq d(x, y) + d(y, z)$ for all $x, y, z \in X$. Obviously, $d_G(u, v)$ is a metric on $V(G)$, and $(V(G), d_G)$ is a metric space called the *graphic metric space* of G. Given a vector space $\mathbb{R}^n$, we can define on it the metric

$$d_{l_1}(x, y) = \sum_{i=1}^{n} |x_i - y_i|$$

for $x, y \in \mathbb{R}^n$. Therefore, $(\mathbb{R}^n, d_{l_1})$ is the l_1-*space*. Since the well-known l_1-space has many excellent properties, we mainly consider embedding the graphic metric space into the l_1-space. At this point, a graph that can be isometrically embedded into the l_1-space is called an l_1-*graph*.

The *n-dimensional hypercube* or *n-cube* Q_n is defined as follows: Let $V_n = \{1, 2, \cdots, n\}$, taking the power set $\mathcal{P}(V_n)$ (the set of all subsets of V_n) as the vertex set, and two vertices A and B are adjacent if and only if $|A\triangle B| = 1$, where $\triangle$ denotes the symmetric difference of two sets A and B, that is, $A\triangle B = (A \setminus B) \cup (B \setminus A)$.

Assouad and Deza [8] showed that a graph G is an l_1-graph if and only if it is scale-λ-embeddable into a hypercube Q_n for some positive integers n and λ, meaning that there exists a mapping φ: $V(G) \to V(Q_n)$ satisfying that

$$\lambda \cdot d_G(x, y)=d_{Q_n}(\varphi(x), \varphi(y))$$

for all $x, y \in V(G)$. The λ is a scale of G. The mapping φ is a *scale-λ-embedding* from G to Q_n. By Shpectorov [9], the minimum scale λ of G is equal to 1 or is even. If $\lambda = 1$, G is called a partial cube. Chepoi, Deza, and Grishukhin [10] showed that every planar l_1-graph has a scale-2-embedding into a hypercube.

In 1973, Djoković [11] characterized that G is a partial cube if and only if G is a connected bipartite graph, and for each adjacent pair u, v in G, $W(u, v) = \{x : d(u, x) < d(v, x)\}$ induces a convex subgraph of G. Blake and Gilchrist [12] proved that the bipartite l_1-graph is a partial cube. Zhang and Wang [13] proved that the graph obtained by gluing two l_1-graphs along one edge is still an l_1-graph if at least one of the two graphs is bipartite. In [14], Wang and Li concluded that the graph obtained by gluing two complete graphs along one edge is an l_1-graph.

A subgraph H of G is an *isometric subgraph* of G if $d_H(u, v) = d_G(u, v)$ for any vertices u, v of H. Suppose that the graph G contains a cycle $C_k = v_0v_1 \cdots v_{k-1}v_0$ for $k \in \mathbb{Z}^+$. Two edges v_iv_{i+1} and v_jv_{j+1} of C_k with $0 \leq i, j < k$ are *opposite* if $d_{C_k}(v_i, v_j) = d_{C_k}(v_{i+1}, v_{j+1})$ is equal to the diameter of C_k, where $v_k = v_0$. When the length k of cycle C_k is even, each edge has a unique opposite edge; if k is odd, each edge has two opposite edges.

In chemical graph theory, a *benzenoid graph* (also known as a *benzenoid system* or *hexagonal system*) refers to a finite connected planar graph without cut vertices, in which each inner surface is bounded by a regular hexagon of edge length 1. The theoretical research on the benzenoid system is very profound. Klavžar et al. [15] showed that any benzenoid graph is a partial cube. In addition,

since a benzenoid graph is a bipartite graph, it is all l_1-graph by [12]. Cyvin et al. [16] provided the definition of a *poly-5-cycle*: a connected system composed of pentagons, where either two pentagons share exactly one edge or they do not intersect. Meanwhile, the degree of the vertices in poly-5-cycles either 2 or 3. Deza and Shtogrin [17] extended this result to a *poly-6-cycle* (a poly-6-cycle refers to a planar graph where the inner vertex degree is 3, the boundary vertex degree is 2 or 3, and all the inner surfaces are hexagons). Deza and Shtogrin [17] confirmed that a poly-5-cycle without dodecahedrons can be embedded in $\frac{1}{2}H_d$. A simple connected poly-6-cycle is also called a benzenoid graph. It follows from the above that the benzenoid graph is an l_1-graph.

A subgraph of a benzene system is called a *coronal benzene system* if the graph G has at least one non-hexagonal interior face (or "hole") and each edge is contained in a hexagon of G. Zhang and Xu [18] demonstrated that the coronoid benzene system cannot be isometrically embedded into Q_n. Zhang and Wang [13] showed that only the $(0, 1)$-type, $(1, 0)$-type, and $(1, 1)$-type open-ended carbon nanotubes (hexagonal tilling into the cylinder) can be isometrically embedded into Q_n.

Fullerenes are 3-regular polyhedral carbon molecules, in which n vertices (i.e., carbon atoms) are arranged in 12 pentagons and $(\frac{n}{2} - 10)$ hexagons. Deza and Grishukhin [19] studied the l_1-embeddedability of fullerene graphs and guessed that only $F_{20}(I_h)$, $F_{26}(D_{3h})$, $F_{44}(T)$, and $F_{80}(I_h)$ are l_1-graphs. Later, Marcusanu [20] pointed out that there are exactly five l_1-embedded fullerene graphs, namely $F_{20}(I_h)$, $F_{26}(D_{3h})$, $F_{40}(T_d)$, $F_{44}(T)$, and $F_{80}(I_h)$. The conditions for l_1-embedding are relaxed so that all vertices whose distances do not exceed integer t can be embedded isometrically into l_1-space, which is called t-embedding. Deza, Fowler, and Shtogrin conducted a comprehensive study in [21] on the t-embeddability of fullerenes generated from icosahedrons and their dual graphs.

In chemical literature, Wiener [22] creatively proposed the concept of a *path number* in 1947. It is mainly used to study the boiling point of paraffin. This is a slightly different but equivalent approach to the *Wiener index*. Hosoya first proposed in [23] to define the Wiener index using the distance between the vertices of the graph. The Wiener index can accurately predict the semiconductor properties of different chiral and ends of pentagon-based nanotubes. This provides a core theoretical basis for the targeted design of high-performance pentagon-based nanotubes for electronic devices, catalysts, and energy storage materials. The Wiener index of graph G is recorded as $W(G)$:

$$W(G) = \frac{1}{2}\sum_{u\in V}\sum_{v\in V} d_G(u, v).$$

Significant progress has been made in the study of the Wiener index in trees (see [24]). For a finite graph G that can be scale-λ-embeddable into a hypercube, let $C(G)$ represent the collection of convex cuts that define this embedding. The number of cuts in $C(G)$ is usually much smaller than the number of pairs (u, v). So, Chepoi et al. [10] proposed another way to calculate the Wiener index:

$$W(G) = \frac{1}{\lambda}\sum_{\{A,B\}\in C(G)} |A||B|.$$

The fastest general algorithm of computing the Wiener index of a graph G, proposed by Mohar and Pisanski [25], is of complexity $O(mn)$, where n and m represent the number of vertices and edges of G, respectively. While when G is an l_1-graph, the complexity of computing the Wiener index can be reduced in linear time [26].

In 1993, Randić [27] proposed a distance-based metric and named it the *hyper-Wiener index*, denoted as WW. The initial definition was only applicable to trees and could not be extended to graphs containing cycles. In 1995, Klein et al. [28] proved that the hyper-Wiener index defined by M. Randić satisfies the following equation:

$$WW(G) = \frac{1}{2} \sum_{\{u,v\} \subseteq V(G)} [d(u,v) + d(u,v)^2].$$

It can be applied to all connected graphs.

In [29], the research results on extremal graphs of distance-based topological indices were reviewed. The extremal graph problems of distance-based topological indices such as the Wiener index, hyper-Wiener index, Harary index, Wiener polarity index, reciprocal complementary Wiener index, and terminal Wiener index were mainly discussed. The topological indexes of the general graph, tree graph, and unicyclic and bicyclic graphs were discussed in detail. Gutman and Trinajstić [30] indicated that the total electronic energy E_π of alternating hydrocarbons is closely related to the sum of the squares of the vertex degrees of the molecular graph. This discovery laid the foundation for the subsequent definition of the first Zagreb index. The first Zagreb index is defined as the sum of the squares of the degrees of all vertices in a graph G (especially a molecular graph) and is denoted as M_1:

$$M_1 = \sum_{v \in V(G)} d(v)^2,$$

where $d(v)$ is vertex degree. The paper [31] laid the theoretical foundation for the second Zagreb index and was denoted as M_2:

$$M_2 = \sum_{uv \in E(G)} d(u)d(v),$$

where $E(G)$ is the set of edges of graph G and $d(u)$ and $d(v)$ are vertex degrees of u and v. Based on the order, the number of leaves, and the domination number of the tree, new upper bounds for the first and second Zagreb indices of the tree were obtained, and the extremal trees that achieve equality in the obtained upper bounds were characterized [32].

Each hexagon in a benzenoid graph contains edges in three directions (see Figure 1). A straight line segment C on a plane is called a *cut segment* if C is perpendicular to one of the three directions of the edge. Both endpoints u and v of C are the centers of an edge, and the graph generated after removing all the edges that intersect C from G has exactly two branches. It also cuts off all the edges that go through C. Take a cut segment in one of three directions and make such a cut segment for each hexagon on the benzenoid graph. Such a planar graph is called a *planar pentagonal system* $\mathcal{P}$ (see Figure 2). Obviously, unlike the poly-5-cycle, $\mathcal{P}$ satisfies the following: (*i*) The degree of the vertices in $\mathcal{P}$ can be 2, 3, or 4, and (*ii*) any two pentagons in $\mathcal{P}$ may share an edge or a vertex, or they may not be adjacent.

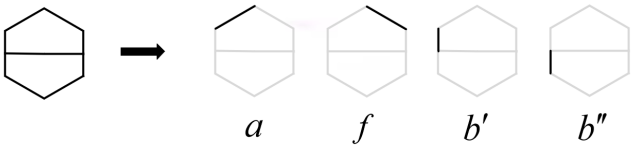

Figure 1. The edges in three directions of the pentagon.

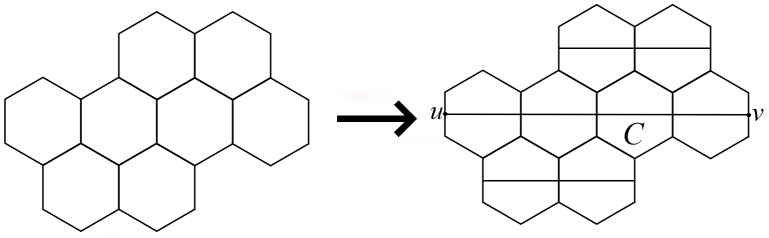

Figure 2. The planar pentagonal system $\mathcal{P}$.

According to [13], select any lattice point in the planar hexagonal lattice as the origin O. $\overrightarrow{a_1}$ and $\overrightarrow{a_2}$ are two unit vectors. The vector $\overrightarrow{OA} = n\overrightarrow{a_1} + m\overrightarrow{a_2}$ satisfies that n and m are two integers and at least one of them is not zero. Add cut segments C in one of three directions to each hexagon of the planar hexagonal lattice.

Draw two lines L_1 and L_2 through O and A, and roll up the pentagons between L_1 and L_2 so that O coincides with A. In this way, a pentagonal tiling $\mathcal{P}$ on the cylinder is obtained. A pentagon-based open-ended nanotube is defined as a finite graph on $\mathcal{P}$ induced by pentagons between c_1 and c_2 (or c_3 and c_4), where c_1 and c_2 (or c_3 and c_4) are two straight lines on $\mathcal{P}$ that do not intersect the vertices around the central axis of the cylinder. The pentagon-based open-ended nanotube is denoted as $\tilde{\mathcal{P}}$. Let c_1 and c_2 (or c_3 and c_4) be the two ends of $\tilde{\mathcal{P}}$; see Figure 3.

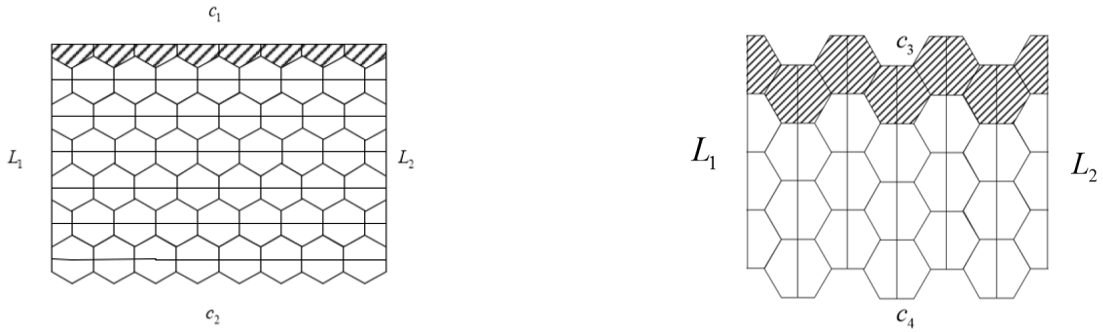

Figure 3. The ends of the pentagon-based nanotubes.

In [13], the open-ended carbon nanotube is denoted as T, and $\overrightarrow{OA}$ is called the chiral vector of T. For any nanotube T, if the chiral vector satisfies $\overrightarrow{OA} = n\overrightarrow{a_1} + m\overrightarrow{a_2}$, T is called the (n, m)-type nanotube. Zigzag nanotubes are $(n, 0)$-type (or $(0, m)$-type) nanotubes. Armchair nanotubes are (n, n)-type nanotubes. In [13], we know that only $(1, 0)$-type, $(0, 1)$-type, and $(1, 1)$-type nanotubes are l_1-graphs. Wang, Xiong, and Chen [33] proved that in the shifted quadrilateral cylinder graph $O_{m,n,k}$, only $O_{m,n,0}$ and $O_{m,3,1}$ are the l_1-graph. Wang and Liu [34] found the explicit closed-form expression for the edge Wiener index of the zigzag nanotubes. According to [35], the Wiener index of the zigzag single-walled carbon nanotube is presented through analytical expressions and recursive formulas. In [36], Wang et al. presented the edge-hyper-Wiener-index of zigzag single-walled nanotubes.

If the cut segment C in the $(n, 0)$-type (or $(0, m)$-type) nanotubes is parallel to $\overrightarrow{a_1}$ (or is parallel to $\overrightarrow{a_2}$), such a cylindrical pentagonal tiling is called a *zigzag pentagon-based nanotube*. We refer to the $(n, 0)$-type nanotube as the *base* of the zigzag pentagon-based nanotube. Similarly, if the cut segment C in the (n, n)-type nanotube is perpendicular to $\overrightarrow{OA}$, such a cylindrical pentagonal tiling is called the

armchair pentagon-based nanotube. We also refer to the armchair nanotube as the *base* of armchair pentagon-based nanotube. In fact, the zigzag pentagon-based nanotubes and the armchair pentagon-based nanotubes are pentagonal tilings on the cylinder surface.

In this paper, we consider the pentagon-based open-ended nanotubes with regular ends (see Figures 4 and 5). According to the shape of the ends, the zigzag pentagon-based nanotubes are represented in three cases; see Figure 4. Similarly, the armchair pentagon-based nanotubes are represented in three cases; see Figure 5. The *cyclic chain* of $\tilde{\mathcal{P}}$ is shown in the shadow in Figure 3. In the unfolded view of the pentagon-based open-ended nanotubes, the shaded area represents a group of pentagonal units connected end-to-end along the circular direction. When the unfolded graph is rolled up along the L_1-L_2 direction into a cylinder, these units form a closed ring. This configuration constitutes the cross-section of the nanotube and is called a cyclic chain. The cyclic chains are the basic units that form the cylindrical structure of the pentagon-based open-ended nanotubes. Let p be the number of the cyclic chains in the pentagon-based nanotubes and q be the number of pentagons in each cyclic chain see Figure 4. Let $I(p, q, \eta)$ be the zigzag pentagon-based nanotubes with both ends being zigzag ends; see Figure 4. Let $I(p, q, \theta)$ be the zigzag pentagon-based nanotubes with only one zigzag end; see Figure 4. Let $I(p, q, \zeta)$ be the zigzag pentagon-based nanotubes with both ends being flat-mouth ends; see Figure 4. Denote $\mathcal{I}(p, q) = \{I(p, q, \eta), I(p, q, \theta), I(p, q, \zeta) : p, q \in Z^+\}$, where η, θ and ζ represent three different types of ends. Let $A(p, q)$ be the armchair pentagon-based nanotubes see Figure 5. Denote $\mathcal{A}(p, q) = \{A(p, q) : p, q \in Z^+\}$.

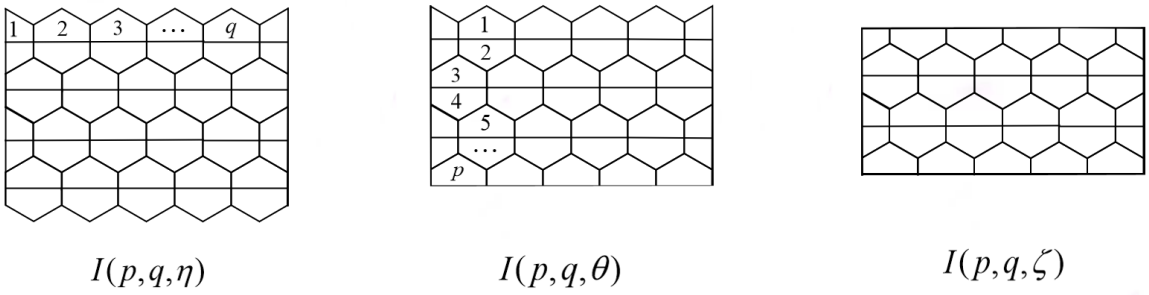

Figure 4. Three types of zigzag pentagon-based nanotubes with different ends.

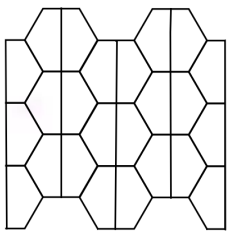

Figure 5. $A(p, q)$.

Theorem 1.1. *Let $\tilde{\mathcal{P}}$ be a pentagon-based open-ended nanotube. Then $\tilde{\mathcal{P}}$ is an l_1-graph if and only if $\tilde{\mathcal{P}}$ is one of pentagon-based nanotubes of the following: $\mathcal{I}(p, 1)$, $\mathcal{I}(1, q, \theta)$ with $q \geq 5$, $I(1, 3, \theta)$, $I(2, 3, \zeta)$, and $I(2, 5, \zeta)$.*

The main contents of this paper are as follows. In Section 2, we study the alternating cuts of

$I(1, q, \theta)$, and we introduce the 5-gonal inequality and the edge labels. In Section 3, the l_1-embeddability of zigzag pentagon-based nanotubes and armchair pentagon-based nanotubes is studied. It has been confirmed that only five types of zigzag pentagon-based nanotubes are l_1-graphs. We also study the Wiener index and hyper-Wiener index of l_1-embeddable $\tilde{\mathcal{P}}$.

2. Materials and methods

2.1. The convex cut

For the planar graph G, the *external face* refers to all the infinitely extended areas that are not surrounded by the graph itself after a planar graph is embedded into the plane. The *boundary edges* of a graph is the set of all the edges contained in the boundaries of its external faces after it is embedded in a plane as a connected planar graph.

Referring tothe description in [10], let G be a finite planar graph. Any partition $C = \{A, B\}$ of the graph G that divides the set of vertices $V(G)$ into two nonempty parts is called a *cut* of G. A cut $\{A, B\}$ of G cuts an edge uv if $u \in A$ and $v \in B$. A subset S of vertices of a graph G is *convex* if for any two vertices u, v of S, all vertices on the shortest u, v-paths belong to S. If both A and B are convex, then the cut $\{A, B\}$ is a *convex cut*. According to [37, 38], it can be known that the l_1-graph can be characterized using the convex cuts:

Theorem 2.1. ([37,38]) *A graph G is scale-λ-embeddable into a hypercube if and only if there exists a collection $C(G)$ of (not necessarily distinct) convex cuts of G such that every edge of G is cut by exactly λ cuts from $C(G)$.*

Lemma 2.1. ([39]) *If a graph G can be scale-λ-embeddable into a hypercube, then for any positive integer r, G can be scale-λr-embeddable into a hypercube.*

For a cut $\{A, B\}$, let $\mathcal{Z}(A, B)$ be the set of inner faces passed by cut $\{A, B\}$ in G, and let $\mathcal{Z}(A, B)$ be the region of cut $\{A, B\}$. Let the boundary of the inner face in G be F, where F is a cycle. Two edges $e'=(u', v')$ and $e''=(u'', v'')$ of F are opposite if $d_G(u', v')=d_G(u'', v'') =D(F)$, where $D(F)$ represents the diameter of F. If F is an even cycle, any edge e in F has exactly one opposite edge. If F is considered to be an odd cycle, then any edge $e \in F$ has two opposite edges e^+ and e^-.

When F is odd, consider dividing the opposite edge of e into left opposite edge e^+ and right opposite edge e^- in clockwise order. If the last turn of the cut in G is to the left, when it reaches the next odd cycle, the turn of this cut is to the right. We say that a cut $\{A, B\}$ is an *opposite cut* of G if each face of $\mathcal{Z}(A, B)$ is cut by cut $\{A, B\}$ from two opposite edges. If the turns on a opposite cut $\{A, B\}$ of planar graph G occur alternately, it is called an *alternating cut*. According to the construction of $\mathcal{P}$, we divide the edges in the pentagon into three directions (see Figure 1). Two alternating cuts are *parallel cuts* if they enter the planar graph $\mathcal{P}$ from a boundary edge in one of the directions and the first turn is the same. It follows from the lemma in [10] that in a planar graph with isometric faces all convex cuts are opposite.

Definition 2.1. *For a cut $\{A, B\}$ in G, sets $A \cap \mathcal{Z}(A, B)$ and $B \cap \mathcal{Z}(A, B)$ are either paths or cycles, denoted as $bd(A)$ and $bd(B)$, and they are called the boundary lines of the cut $\{A, B\}$.*

According to the properties of the subgraph, for any two vertices in subgraph H, there are $d_H(x, y) \geq d_G(x, y)$. If G is an l_1-graph, then obviously the following proposition is true:

Proposition 2.1. *Any isometric subgraph of the l_1-graph is still an l_1-graph.*

We stipulate that all cuts in this paper should start from the boundary edges.

2.2. The 5-gonal inequality

Regarding the l_1-embeddability of the graph, a necessary condition is also given in [40]. We describe it in the following lemma:

Lemma 2.2. ([40]) *If graph G is an l_1-graph, then d_G must satisfy the 5-gonal inequality: any five vertices x, y, a, b, and c of G (see Figure 6), there is*

$$d(x,y) + (d(a,b) + d(a,c) + d(b,c)) \leq (d(x,a) + d(x,b) + d(x,c)) + (d(y,a) + d(y,b) + d(y,c)).$$

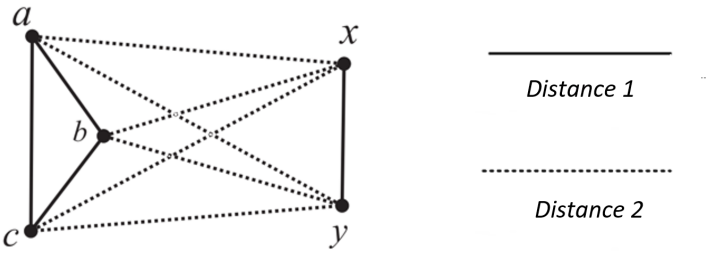

Figure 6. The 5-gonal inequality.

2.3. The edge labels

An edge label of the l_1-graph was first mentioned in [9]. Let G be a finite l_1-graph and φ be scale-λ-embedding of G into Q_n. Assign a label $l(uv)$ to each edge $e = uv$ of G as follows: $l(uv) = \varphi(u) \triangle \varphi(v)$. As pointed out in [9], each edge is labeled with exactly λ elements of set V_n:

$$|l(uv)| = |\varphi(u) \triangle \varphi(v)| = d_{Q_n}(\phi(u), \phi(v)) = \lambda \cdot d_G(u,v) = \lambda.$$

Regarding the edge labels on the path, we have the following lemmas:

Lemma 2.3. ([20,41]) *Let v_0, v_n be two vertices of an l_1-graph G, and ϕ be a scale-λ-embedding of G into a hypercube, then the following holds:*

(1) If $\gamma = v_0 v_1 \cdots v_n$ is a path from v_0 to v_n, then $\phi(v_0) \triangle \phi(v_n) = l(v_0v_1) \triangle \cdots \triangle l(v_{n-1}v_n)$.

(2) If γ is a shortest path, the labels $l(v_0v_1), l(v_1v_2), \cdots, l(v_{n-1}v_n)$ are pairwise disjoint and $\phi(v_0) \triangle \phi(v_n) = l(v_0v_1) \cup l(v_1v_2) \cup \cdots \cup l(v_{n-1}v_n)$.

In particular, the label of each edge on any shortest path from v_0 to v_n is included in $\phi(v_0) \triangle \phi(v_n)$.

Lemma 2.4. ([41,42]) *Suppose C_k is an isometric cycle in l_1-graph G uv and xy are a pair of opposite edges of C_k.*

(1) If k is even, then $l(uv) = l(xy)$.

(2) If k is odd, then $|l(xy) \cap l(uv)| = \frac{\lambda}{2}$. Furthermore, if vw is the other opposite edge of xy, then $l(xy) \subset l(uv) \cup l(vw)$.

In cycle C_k, the labels of edges that are not opposite are all disjoint.

3. The results and discussion

3.1. l_1-embeddability of zigzag pentagon-based nanotubes

When $p = 1$, we consider that the pentagon-based nanotubes are zigzag pentagon-based nanotubes. The obtained zigzag pentagon-based nanotubes are pressed onto the plane to form a planar graph with an *n-gon* in the middle, and each edge of the *n-gon* extends outward to form a pentagon. According to the research of Deza and Shtogrin [17] in 2000, the zigzag pentagon-based nanotubes at $p = 1$ can be called *mono-n-5-cycle*, and all of the inner surfaces are pentagons except for one *q-gon* (see Figure 7). When $q \geq 5$, we look for the collection $C(I(1, q, \theta))$ of alternating cuts of $I(1, q, \theta)$. Let's assume that all the pentagons in $I(1, q, \theta)$ are P^{1*}.

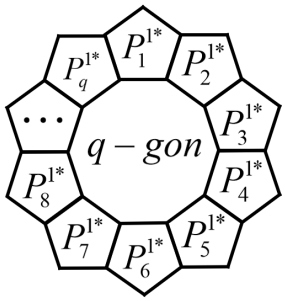

Figure 7. $I(1, q, \theta)$.

Entering from the boundary edges of the zigzag pentagon-based nanotubes $I(1, q, \theta)$, we can obtain the alternating cuts of $I(1, q, \theta)$ as shown in Figure 8. It can be found that for any q, the a-left cut, a-right cut, f-left cut, f-right cut, and their parallel cuts constitute the collection $C(I(1, q, \theta))$ of alternating cuts of $I(1, q, \theta)$.

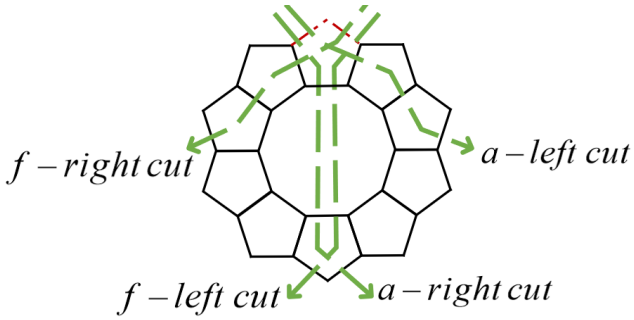

Figure 8. The collection of alternating cuts of $I(1, q, \theta)$.

Since $I(1, q, \theta)$ is composed of q pentagons and a q-polygon, each side of the pentagon has two opposite sides, while each side of the q-polygon has either one or two opposite sides. Therefore, the collection $C(I(1, q, \theta))$ of alternating cuts can cut the edges of all the inner faces of $I(1, q, \theta)$ twice.

After completing the construction and analysis of the collection $C(I(1, q, \theta))$ of alternating cuts, we can obtain the following proposition about convex cuts:

Proposition 3.1. *If $q \geq 5$, any alternating cuts of $I(1, q, \theta)$ are convex cuts.*

Proof. When $q \geq 5$, the inner surfaces that a-left cut and f-right cut pass are pentagons.

The a-left cut divides the graph into two parts A_1 and B_1, denotting the a-left cut as cuts $\{A_1, B_1\}$ (see Figure 9). For any cut $\{A_1, B_1\}$, by removing all the edges in $\mathcal{Z}(A_1, B_1)$ that intersect with the cut $\{A_1, B_1\}$, two connected components of $I(1, q, \theta)$ can be obtained. The connected component is a path with endpoints on B_1. According to [43], for any two vertices x and y on B_1, there exists a unique shortest path.

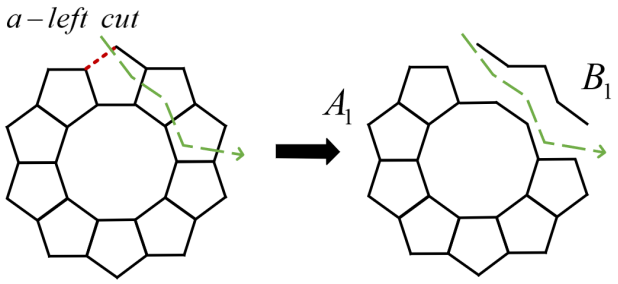

Figure 9. The a-left cut in $I(1, 10, \theta)$.

Suppose the a-left cut and f-right cut are not the convex cuts of $I(1, q, \theta)$. The region passed by the a-left cut is marked as $\mathcal{Z}(A_1, B_1)$. $I(1, q, \theta)$ is divided into two parts by $\mathcal{Z}(A_1, B_1)$. Let the subgraph on the left of $\mathcal{Z}(A_1, B_1)$ be A_1 and the subgraph on the right be B_1. There must exist cut $\{A_1, B_1\}$ such that for two vertices $x,\ y \in A_1$, there is a shortest path P between x and y satisfying $P \cap B_1 \neq \emptyset$. Suppose that among all the vertices in A_1 that violate convexity, $x,\ y$ get as close as possible.

Let x' and y' be the adjacent vertices of x and y in P, respectively, and x', y' and all the vertices in P that are between x' and y' belong to B_1. Both xx' and yy' are cut by $\{A_1, B_1\}$, $x, y \in A_1$, $x', y' \in B_1$. Thus,

$$d_{bd(A_1)}(x, y) = d_P(x, y),\ d_{bd(B_1)}(x', y') = d_P(x', y').$$

The properties of alternating cut and pentagon are

$$|d_{bd(A_1)}(x, y) - d_{bd(B_1)}(x', y')| \leq 1.$$

So,

$$d_{bd(B_1)}(x', y') + 2 > d_{bd(A_1)}(x, y).$$

We can replace the x, y-path in P with the x, y-path in A_1, so we get a shorter path. The above text, the assumption does not hold. So, the a-left cut and f-right cut are convex cuts.

Consider the a-right cut. The region passed by the a-right cut is marked as $\mathcal{Z}(A, B)$. $I(1, q, \theta)$ is divided into two parts by $\mathcal{Z}(A, B)$. Let the subgraph on the left of $\mathcal{Z}(A, B)$ be A and the subgraph on the right be B.

By contradiction, suppose A is not convex, then it exists $u, v \in A$ such that there is the shortest path P^* between u and v satisfying $P \cap B \neq Q$ (see Figure 10). Find vertices x and y in P, and x' and y' are their adjacent vertices, respectively. yy' is the edge that is closest to v among all the edges cut by the a-right cut, and xx' is closer than edge yy'. Obviously x', y' are the neighbors of x, y and $x, y \in bd(A)$, $x', y' \in bd(B)$. Since $\mathcal{Z}(A, B)$ is composed of P^* and q-gon, there is

$$|d_{bd(A)}(x, y) - d_{bd(B)}(x', y')| \leq 1.$$

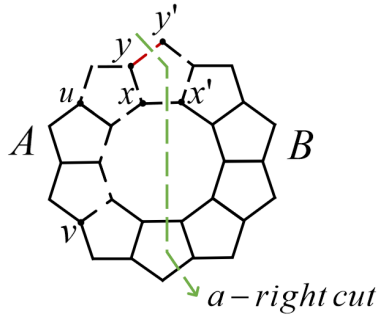

Figure 10. The u, v-path in $I(1, 10, \theta)$.

It can be expanded from the equation to obtain

$$d_{bd(B)}(x', y') - 1 \leq d_{bd(A)}(x, y) \leq d_{bd(B)}(x', y') + 1 < d_{bd(B)}(x', y') + 2.$$

We replace the x, y-path in P with the x, y-path in A, so we get a shorter u, v-path. Therefore, the assumption does not hold, and the a-right cut is a convex cut. Similarly, it can be concluded that the f-left cut is also a convex cut.

Therefore, when $q \geq 5$, the collection $C(I(1, q, \theta))$ of alternating cuts is the collection of convex cuts. □

Theorem 3.1. *Let $\tilde{\mathcal{P}}$ be in $\mathcal{I}(1, q, \theta)$. Then $\tilde{\mathcal{P}}$ is an l_1-graph if and only if $\tilde{\mathcal{P}}$ is in $\mathcal{I}(1, q, \theta)$ with $q \neq 2$ or $q \neq 4$.*

Proof. When $q = 1$, the zigzag pentagon-based nanotube $\tilde{\mathcal{P}}$ is cut along a line parallel to the central axis of $\tilde{\mathcal{P}}$ (see Figure 11). Since the appearance of self-loops and multiple edges in the l_1-graph does not affect the distance between vertices, $I(1, 1, \theta)$ is isomorphic to a binary long path. In 1994, Deza and Laurent [44] indicated that the path is an l_1-graph.

Figure 11. Sectioning chart and cylindrical chart of $I(1, 1, \theta)$.

When $q = 3$, we utilize the recognition algorithm of l_1-graphs described in [45]. It is found that $I(1, 3, \theta)$ can be scale-2-embeddable into Q_7. The vertex label is given in Figure 12.

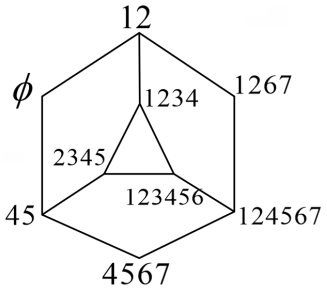

Figure 12. The vertex label of $I(1, 3, \theta)$.

When $q = 2$ or 4, there are five vertices in the graphs that violate the 5-gonal inequality (see Figure 13).

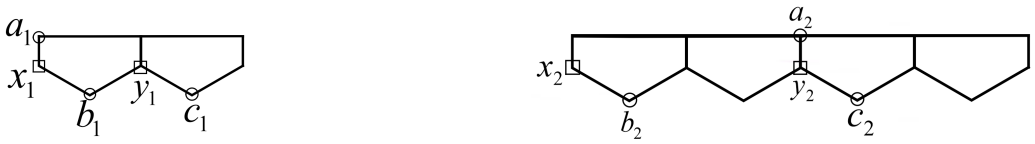

Figure 13. The vertices in $I(1, 2, \theta)$ and $I(1, 4, \theta)$ that violate the 5-gonal inequality.

In $I(1, 2, \theta)$, $(d(a_1, b_1) + d(a_1, c_1) + d(b_1, c_1)) + d(x_1, y_1)=(2 + 2 + 2) + 2 = 8$, while

$$(d(x_1, a_1) + d(x_1, b_1) + d(x_1, c_1)) + (d(y_1, a_1) + d(y_1, b_1) + d(y_1, c_1)) = (1 + 1 + 1) + (2 + 1 + 1) = 7.$$

In $I(1, 4, \theta)$, $(d(a_2, b_2) + d(a_2, c_2) + d(b_2, c_2)) + d(x_2, y_2)=(3 + 2 + 4) + 4 = 13$, while

$$(d(x_2, a_2) + d(x_2, b_2) + d(x_2, c_2)) + (d(y_2, a_2) + d(y_2, b_2) + d(y_2, c_2))=(3 + 1 + 3) + (1 + 3 + 1) = 12.$$

The vertices a_1, b_1, c_1, x_1, y_1 and a_2, b_2, c_2, x_2, y_2 violate the 5-gonal inequality in $I(1, 2, \theta)$ and $I(1, 4, \theta)$. Obviously $I(1, 2, \theta)$ and $I(1, 4, \theta)$ are not l_1-graphs.

Combined with Theorem 2.1 and Proposition 3.1, $I(1, q, \theta)$ with $q \geq 5$ is an l_1-graph. □

Proposition 3.2. *The pentagonal chain $H = I(2, q, \zeta)$ is an isometric subgraph of $I(p, q)$ with $p \geq 2$.*

Proof. When $p = 2$, H is just $I(2, q, \zeta)$ itself. Clearly, H is an isometric subgraph of $I(2, q, \zeta)$.

When $p > 2$, we prove by contradiction that c is an isometric cycle of H. Suppose c is not an isometric cycle of H, then there exists x and y belonging to c such that $d_c(x, y) > d_H(x, y)$. Find a shortest path P between x and y, $d_H(x, y) = |P|$. Let P have t intersections with c, and let $x = x_0$, $y = x_{t+1}$. Select the shortest path $P_{x_i x_{i+1}}$ that falls completely within H between intersections x_i and x_{i+1} $0 \leq i \leq t$. Let $d_c(x_i, x_{i+1}) = k$, according to the structure of the pentagon:

$$\begin{cases} 2k + 2 \leq |P_{x_i x_{i+1}}| \leq k + 5, & k \leq 3, \\ k + 5 \leq |P_{x_i x_{i+1}}| \leq 2k + 2, & k > 3. \end{cases} \tag{3.1}$$

Obviously, replacing $P_{x_i x_{i+1}}$ with the x_i, x_{i+1}-path on c can yield a shorter path $x - P - x_i - P'_{x_i x_{i+1}} - x_{i+1} - P - y$ between x and y. So,

$$\sum_{i=0}^{t+1} d_c(x_i, x_{i+1}) < d_H(x, y) = |P|,$$

which contradicts the contradiction that P is the shortest path between x and y. Therefore, c is an isometric cycle of H.

Cycle c divides $I(p,q)$ into two parts and considers the parts that intersect with it. Let one part be T_1 and the other part be T_2. Similarly, c is also an isometric cycle of T_2 and $I(p,q)$. For any two vertices u and v on cycle c, there are $d_c(u,v) = d_H(u,v) = d_{T_1}(u,v) = d_{T_2}(u,v) = d_{I(p,q)}(u,v)$. Next we take any two vertices x and y in H and show that H is an isometric graph of $I(p,q)$. Find a shortest path P between x and y.

Discuss the position of P in different situations:

Case 1: $P \in H$, $d_H(x,y) = d_G(x,y)$.

Case 2: P does not entirely belong to H.

Let us assume $P \cap T_2 \neq \varnothing$. Therefore, P and c must have the intersection vertices, and the distance from the intersection vertices to x are denoted as $x_1, x_2, \cdots, x_g$, $g \in N^+$. In this case, we can write P as $P = P_{xx_1} + P_{x_1x_2} + \cdots + P_{x_gy}$. Since c is an isometric cycle of $I(p,q)$, there $d_c(x_1,x_2) = d_P(x_1,x_2)$, $d_c(x_2,x_3) = d_P(x_2,x_3)$, $\cdots$, and $d_c(x_{g-1},x_g) = d_P(x_{g-1},x_g)$. Rewrite P as P': $P' = P_{xx_1} + c_{x_1x_2} + c_{x_2x_3} + \cdots + c_{x_{g-1}x_g} + P_{x_gy}$ P' is completely in H. Since $H \subseteq I(p,q)$, by properties of the subgraph and the above proof, it can be seen that $d_H(x,y) = d_{I(p,q)}(x,y)$. H is the isometric subgraph of $I(p,q)$ (see Figure 14). □

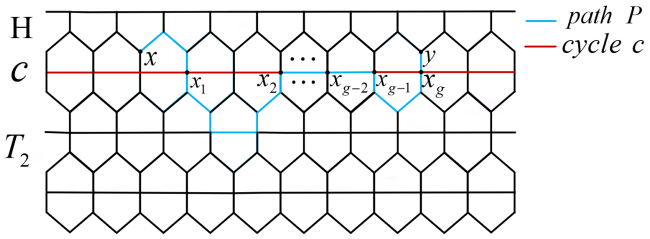

Figure 14. The x,y-path *in* $I(7,q,\theta)$.

According to Proposition 3.2, it can be obtained that the pentagonal chain H' of the shape $I(3,q,\theta)$ located at the zigzag end is also an isometric subgraph of the zigzag pentagon-based nanotubes $I(p,q,\eta)$ and $I(p,q,\theta)$ with $p \geq 3$ (see Figure 15).

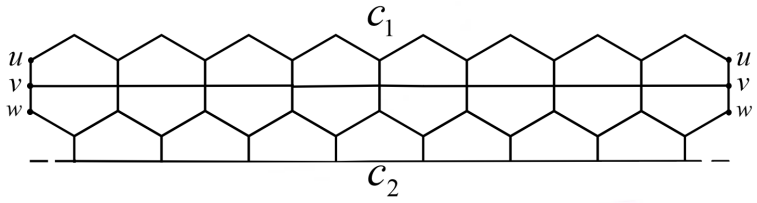

Figure 15. The pentagonal chain H'.

Theorem 3.2. *Let $\tilde{\mathcal{P}}$ be in $\mathcal{I}(p,q,\eta) \cup \mathcal{I}(p,q,\theta)$. Then $\tilde{\mathcal{P}}$ is an l_1-graph if and only if $\tilde{\mathcal{P}}$ is in $\mathcal{I}(p,1,\eta) \cup \mathcal{I}(p,1,\theta)$ with $p \geq 2$.*

Proof. When $p \geq 2$, $q = 1$. As stated in Theorem 3.1, $I(p,1)$ is isomorphic to the path, so obviously it is the l_1-graph.

When $p \geq 3$, $q \geq 2$, the pentagonal chain H' satisfying Proposition 3.2 is the isometric subgraphs of $I(p, q)$. Let the two ends of H' be c_1 and c_2, respectively. Name the pentagonal chain at the zigzag end in H' as H'_1, and name the chain composed of the pentagons that share edge c_i with pentagons in H'_1 as H'_2. Let the pentagons in H'_1 and H'_2 be $H'_{1,1}, H'_{1,2}, \cdots, H'_{1,q}$ and $H'_{2,1}, H'_{2,2}, \cdots, H'_{2,q}$, $q \geq 2$, respectively. $H'_{p,i}$ is adjacent to $H'_{p,i-1}$ and $H'_{p,i+1}$ (i is modulo n). Suppose $H'_{1,1}$ and $H'_{1,q}$ share edge uv, and $H'_{2,1}$ and $H'_{2,q}$ share edge vw, where

$$u = H'_{1,1} \cap H'_{1,q} \cap c_1, \quad v = H'_{2,1} \cap H'_{2,q} \cap c_2.$$

Similar to [13], we solve the problem with the 5-gonal inequality.

Case 1: In Figure 16, q is even. Let $a = H'_{1,1} \cap c_1$ satisfy

$$d_H(a) = 2, \quad x = H'_{2,\frac{q}{2}} \cap H'_{2,\frac{q+1}{2}+1}$$

with $d_H(x) = 3$. b is the adjacent vertex of x in $H'_{2,\frac{q}{2}+1}$ with

$$d_H(b) = 3, \quad y = H'_{1,\frac{q}{2}+1} \cap H'_{1,\frac{q}{2}+2} \cap c_1,$$

and c is the adjacent vertex of y in $H'_{1,\frac{q}{2}+1} \cap c_1$.

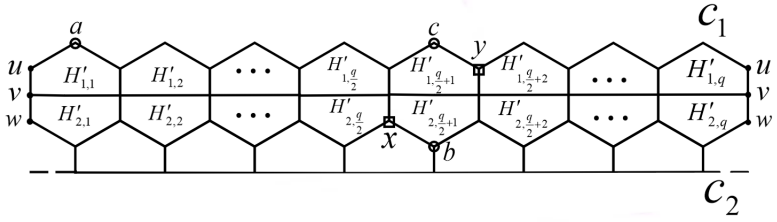

Figure 16. q is even.

When $2 \leq q \leq 6$, $(d(a, b) + d(a, c) + d(b, c)) + d(x, y) = (\frac{n}{2} + n + 4) + 3 = \frac{3q}{2} + 10$, while

$$(d(x, a) + d(x, b) + d(x, c)) + (d(y, a) + d(y, b) + d(y, c)) = (\tfrac{q}{2} + 2 + 1 + 3) + (q - 1 + 3 + 1) = \tfrac{3q}{2} + 9.$$

When $q \geq 8$, $(d(a, b) + d(a, c) + d(b, c)) + d(x, y) = (q - 1 + q - 1 + 4) + 3 = 2q + 5$, while

$$(d(x, a) + d(x, b) + d(x, c)) + (d(y, a) + d(y, b) + d(y, c)) = (q - 2 + 1 + 3) + (q - 2 + 3 + 1) = 2q + 4.$$

When q is an even number, there are always five vertices that violate the 5-gonal inequality.

Case 2: In Figure 17, q is odd. Select w in $H'_{2,1}$ as a,

$$x = H'_{2,\frac{q-1}{2}} \cap H'_{2,\frac{q+1}{2}}$$

with $d_H(x) = 3$. b is the adjacent vertex of x in $H'_{2,\frac{q+1}{2}}$ with

$$d_H(b) = 3, \quad y = H'_{1,\frac{q+1}{2}} \cap H'_{1,\frac{q+1}{2}+1} \cap c_1,$$

and x is the adjacent vertex of y in $H'_{1,\frac{q+1}{2}} \cap c_1$.

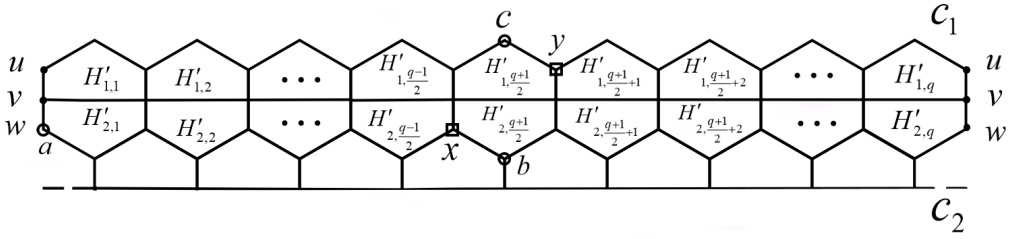

Figure 17. q is odd.

When $q = 3$, $(d(a,b) + d(a,c) + d(b,c)) + d(x,y) = (3 + 4 + 4) + 3 = 14$, while

$$(d(x,a) + d(x,b) + d(x,c)) + (d(y,a) + d(y,b) + d(y,c)) = (2 + 1 + 3) + (3 + 3 + 1) = 13.$$

When $q \geq 5$, $(d(a,b) + d(a,c) + d(b,c)) + d(x,y) = (\frac{q+5}{2} + 4 + \frac{q+5}{2}) + 3 = q + 12$, while

$$(d(x,a) + d(x,b) + d(x,c)) + (d(y,a) + d(y,b) + d(y,c)) = (\tfrac{q+3}{2} + 1 + 3) + (\tfrac{q+3}{2} + 1 + 3) = q + 11.$$

When q is an odd number, there are always five vertices that violate the 5-gonal inequality.

When $p = 2$ and $q \geq 2$, there are five vertices at the same position in $I(2, q, \eta)$ that violate the pentagonal inequality.

From the above expressions and Lemma 2.2, it follows that the pentagonal chain H' is not an l_1-graph. In combination with Proposition 2.1, the theorem is proved. □

Theorem 3.3. *$I(p, q, \zeta)$ is an l_1-graph if and only if $p \geq 2$ and $q = 1$, or $p = 2$ and $q = 3$ or 5.*

Proof. When $q = 1$, as proved in Theorem 3.1, $I(p, 1, \zeta)$ is isomorphic to the path P, which is an l_1-graph.

When $q = 2$, Figure 18 is an isometric subgraph of $I(p, 2, \zeta)$ ($p \geq 2$) by Proposition 3.2. There are five vertices a_2, b_2, c_2, x_2, y_2 in Figure 18 that violate the 5-gonal inequality:

$$(d(a_2, b_2) + d(a_2, c_2) + d(b_2, c_2)) + d(x_2, y_2) = 8,$$

while

$$(d(x_2, a_2) + d(x_2, b_2) + d(x_2, c_2)) + (d(y_2, a_2) + d(y_2, b_2) + d(y_2, c_2)) = 7.$$

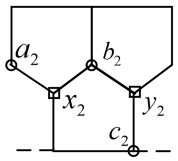

Figure 18. Forbidden isometric subgraph of $I(p, 2, \zeta)$.

When $q = 3$ and $p = 2$, according to the recognition algorithm of the l_1-graph, $I(2, 3, \zeta)$ can be scale-2-embeddable into Q_8. The vertex labels are given below (see Figure 19):

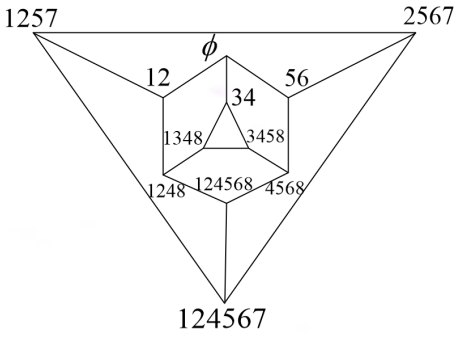

Figure 19. The vertex labels of $I(2, 3, \zeta)$.

When $q = 3$ with $p \geq 4$, we can still find five vertices a', b', c', x', y' in Figure 20 that violate the 5-gonal inequality. According to Proposition 3.2, Figure 20 is the isometric subgraph of $I(p, 3, \zeta)$ $(p \geq 4)$: $(d(a' + b') + d(a' + c') + d(b' + c')) + d(x' + y') = 14$, while

$$(d(x' + a') + d(x' + b') + d(x' + c')) + (d(y' + a') + d(y' + b') + d(y' + c')) = 13.$$

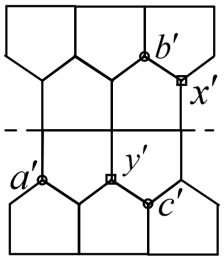

Figure 20. Forbidden isometric subgraph of $I(p, 3, \zeta)$, $p \geq 4$.

When $q = 4$, it can be known from Proposition 3.2 that Figure 21 is an isometric subgraph of $I(p, 4, \zeta)$ $(p \geq 2)$. Finding five vertices a_4, b_4, c_4, x_4, y_4 in Figure 21 violates the 5-gonal inequality: $(d(a_4, b_4) + d(a_4, c_4) + d(b_4, c_4)) + d(x_4, y_4) = 13$, while

$$(d(x_4, a_4) + d(x_4, b_4) + d(x_4, c_4)) + (d(y_4, a_4) + d(y_4, b_4) + d(y_4, c_4)) = 12.$$

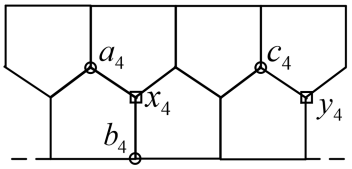

Figure 21. Forbidden isometric subgraph of $I(p, 4, \zeta)$.

When $q = 5$ with $p = 2$, it is shown in [21], the dodecahedron $I(2, 5, \zeta)$ has been obtained as an l_1-graph.

When $q = 5$ with $p = 3$, $I(3, 5, \zeta)$ is in fact the nanotube $I(3, 5, \theta)$, as shown in Theorem 3.2, and it is not an l_1-graph.

When $q = 5$ with $p \geq 4$, we can still find five vertices a_5, b_5, c_5, x_5, y_5 in Figure 22 that violate the 5-gonal inequality. According to Proposition 3.2, Figure 22 is the isometric subgraph of $I(p, 5, \zeta)$ $(p \geq 4)$: $(d(a_5 + b_5) + d(a_5 + c_5) + d(b_5 + c_5)) + d(x_5 + y_5) = 17$, while,

$$(d(x_5 + a_5) + d(x_5 + b_5) + d(x_5 + c_5)) + (d(y_5 + a_5) + d(y_5 + b_5) + d(y_5 + c_5)) = 16.$$

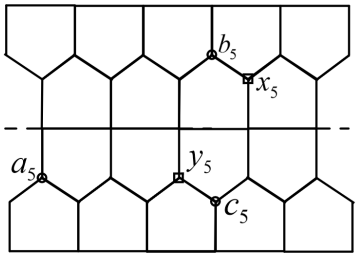

Figure 22. Forbidden isometric subgraph of $I(4, 5, \zeta)$, $p \geq 4$.

When $q = 6$, similarly Figure 23 is an isometric subgraph of $I(p, 6, \zeta)$ $(p \geq 2)$. Five vertices a_6, b_6, c_6, x_6, y_6 can also be found to prove that Figure 23 violates the 5-gonal inequality: $(d(a_6, b_6) + d(a_6, c_6) + d(b_6, c_6)) + d(x_6, y_6) = 16$, while

$$(d(x_6, a_6) + d(x_6, b_6) + d(x_6, c_6)) + (d(y_6, a_6) + d(y_6, b_6) + d(y_6, c_6)) = 15.$$

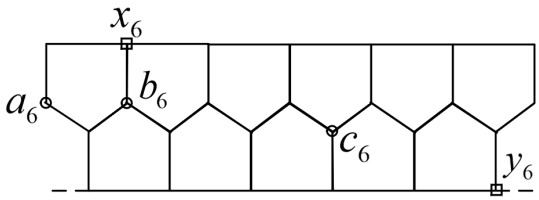

Figure 23. Forbidden isometric subgraph of $I(p, 6, \zeta)$.

When $q \geq 7$, from Proposition 3.2, it can be known that Figure 24 is a forbidden subgraph of the embeddable hypercube of the mono-q-5-cycle: $(d(x, y) + d(a, b) + d(a, c)) + d(b, c) = 16$, while

$$(d(x, a) + d(x, b) + d(x, c)) + (d(y, a) + d(y, b) + d(y, c)) = 15.$$

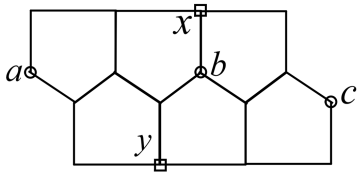

Figure 24. Forbidden isometric subgraph of $I(p, 7, \zeta)$, $(p \geq 2, q \geq 7)$.

Based on the above proofs, Proposition 2.1, and Lemma 2.2, it can be known that the zigzag pentagon-based nanotubes $\mathcal{I}(p, 1)$, $\mathcal{I}(1, q, \theta)$ with $q \geq 5$, $I(1, 3, \theta)$, $I(2, 3, \zeta)$, and $I(2, 5, \zeta)$ are l_1-graphs.

This completes the proof. □

3.2. l_1-embeddability of armchair pentagon-based nanotubes

For armchair pentagon-based nanotube $A(p, q)$, when q is odd or $\frac{q}{2}$ is an odd number, it cannot be seamlessly spliced into pentagon-based nanotubes (see Figure 25). Therefore, only the case where both q and $\frac{q}{2}$ are even numbers and $q \geq 4$ is considered.

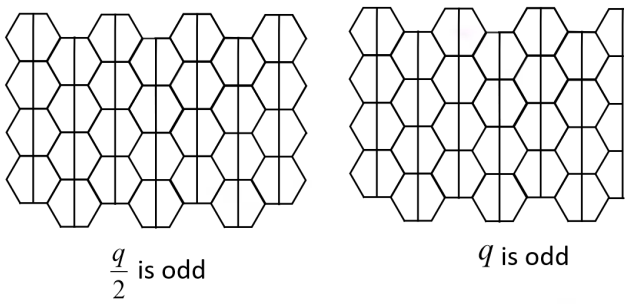

Figure 25. $A(p, q)$ when q and $\frac{q}{2}$ are odd numbers.

Proposition 3.3. *In $A(p, q)$, each cyclic chain is isometric.*

Proof. By contradiction, suppose cyclic chain M is not an isometric subgraph of $A(p, q)$, then there exist two vertices u, v ($d_{A(p,q)}(u, v)$ should be as small as possible) in M such that their distance in $A(p, q)$ is smaller than that in M, i.e.,

$$d_{A(p,q)}(u, v) < d_M(u, v). \tag{3.2}$$

Let $P = uu_1u_2 \cdots u_lv$ be the shortest path that satisfies the above conditions and $u_1u_2 \cdots u_l \in V(A(p, q)) \setminus V(M)$. Otherwise, for $u_i \in V(M)$ $(1 \leq i \leq l)$, $uu_1u_2 \cdots u_i$ and $u_iu_{i+1} \cdots u_lv$ satisfy $d_M(u, u_i) \geq d_{A(p,q)}(u, u_i)$ and $d_M(u_i, v) \geq d_{A(p,q)}(u_i, v)$, and one of them is strictly true. This contradicts the minimality of $d_{A(p,q)}(u, v)$.

Let Q be the shortest path between u and v in M, which is entirely contained within M and $|Q| = d_M(u, v)$. From Eq (3.2), it follows that $|P| < |Q|$. O is a subgraph of $A(p, q)$ formed by $P \cup Q$ and its internal faces (see Figure 26). Since $P \cup Q$ is a simple closed cycle in $A(p, q)$ according to the Jordan curve theorem, this closed cycle divides $A(p, q)$ into two regions: the interior and the exterior. O is the subgraph formed by all the vertices, edges, and pentagonal faces within the interior of the closed cycle. Since $A(p, q)$ contains only pentagonal faces and has no cycles with lengths less than 5 and M has no chords, O is a simply connected planar graph consisting only of pentagons and without internal cycles. Thus, O must be a pentagonal chain. In O, there exists a sequence of pentagons: $H_1, H_2, \cdots, H_k$. The adjacent pentagons H_i and H_{i+1} share one edge, and two non-adjacent pentagons have no common edges. u is a vertex in H_1, and v is a vertex in H_k. Q is the shortest path between u and v that is completely within M, and it shares at most two edges adjacent to vertex u with pentagon H_1. P is the shortest path between u and v located outside M, forming the boundary of O and sharing at least 2 edges with H_1. Similarly, it can be concluded that H_k shares at most 2 edges with Q and at least 2 edges with P. Therefore, the pentagons H_1 and H_k contribute at most 4 edges to Q and at least 4 edges to P.

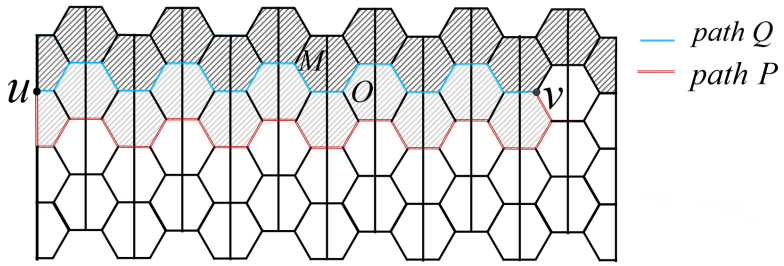

Figure 26. P, Q, O, and M in $A(4, 24)$.

For the pentagons H_i (where $1 \leq i \leq k-1$), in the pentagonal chain, it only shares one edge with each of the adjacent left and right pentagons. The remaining 4 edges respectively belong to the boundaries P and Q of O. According to the symmetry of the armchair pentagon-based nanotubes, we can obtain: $|P \cap O| = |Q \cap O|$. Therefore, $|P| \geq |Q|$ contradicts the inequality (3.2).

Taking the above proof together, it can be obtained that the cyclic chain M is the isometric graph of the armchair pentagon-based nanotube $A(p, q)$. □

Theorem 3.4. *Any armchair pentagon-based nanotube $A(p, q)$ is not an l_1-graph.*

Proof. When $p = 1$, the cyclic chain M is $A(1, q)$. Let the pentagons in the cyclic chain M be M_1, M_2, $\cdots$, M_q with $q \geq 4$, where M_i is adjacent to M_{i-1} and M_{i+1}. Let M_1 and M_q share an edge uv, u=$M_1 \cap M_q \cap c_3$, v=$M_1 \cap M_q \cap c_4$ (c_3 and c_4 are ends of M).

Assume that a is a vertex obtained from $M_1 \cap M_2 \cap c_3$. c is a vertex whose degree is 2 in $M_{\frac{q}{2}+1} \cap c_4$, and c is a vertex in $M_{\frac{q}{2}+1} \cap M_{\frac{q}{2}+2} \cap c_3$. x is a vertex of $M_{\frac{q}{2}} \cap M_{\frac{q}{2}+1} \cap c_3$, and y is a vertex in $M_{\frac{q}{2}+1} \cap M_{\frac{q}{2}+2} \cap c_4$. In Figure 27, there are five vertices that violate the pentagon inequality.

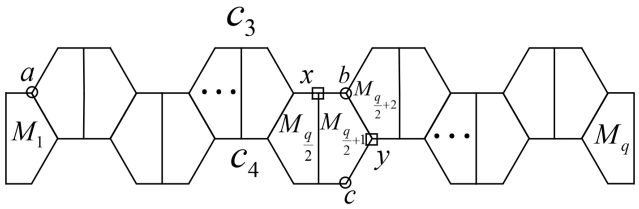

Figure 27. M that violates the 5-gonal inequality.

$$(d(a,b) + d(a,c) + d(b,c)) + d(x,y) = (\tfrac{3q}{2} + \tfrac{3q}{2} + 2) + 2 = 3q + 4,$$

while

$$(d(x,a) + d(x,b) + d(x,c)) + (d(y,a) + d(y,b) + d(y,c)) = (\tfrac{3q}{2} - 1 + 1 + 2) + (\tfrac{3q}{2} - 1 + 1 + 1) = 3q + 3.$$

According to Lemma 2.2, M is not an l_1-graph. Based on Propositions 2.1 and 3.3, it can be known that $A(p, q)$ is not an l_1-graph. □

All propositions and theorems have been proved. The core theorem of this paper is concluded as follows:

Theorem 1.1. *Let $\tilde{\mathcal{P}}$ be a pentagon-based open-ended nanotube. Then $\tilde{\mathcal{P}}$ is an l_1-graph if and only if $\tilde{\mathcal{P}}$ is one of pentagon-based nanotubes of the following: $\mathcal{I}(p, 1)$, $\mathcal{I}(1, q, \theta)$ with $q \geq 5$, $I(1, 3, \theta)$, $I(2, 3, \zeta)$, and $I(2, 5, \zeta)$.*

Proof. It can be proved from Theorems 3.1–3.4. □

3.3. The chemical indices of l_1-embeddable pentagon-based open-ended nanotubes

Given the significance of pentagon-based open-ended nanotubes in chemical graph theory and materials science, we further investigate the calculation of their chemical indices. In this section, we present all the chemical indices of the l_1-embeddable $\tilde{\mathcal{P}}$.

3.3.1. The Wiener index of l_1-embeddable pentagon-based open-ended nanotubes

Theorem 3.5. *When $p \geq 1$, the Wiener index of $I(p, 1)$ is*

$$W(I(p,1)) = \begin{cases} \binom{\frac{3p}{2}+2}{3}, & p > 1 \text{ and } p \text{ is even}; \\ \binom{\frac{3p+3}{2}}{3}, & p \geq 1 \text{ and } p \text{ is odd}. \end{cases} \tag{3.3}$$

Proof. In [46], the Wiener index of the path P_n with $n \geq 3$ has a specific calculation formula:

$$W(P_n) = \binom{n+1}{3}. \tag{3.4}$$

From the proof processes of Theorems 3.2 and 3.3, it can be known that when $p \geq 1$ and is an even number, $I(p, 1)$ is isomorphic to the path $P_{\frac{3p}{2}+2}$; when $p \geq 1$ and is an odd number, $I(p, 1)$ is isomorphic to the path $P_{\frac{3p+3}{2}}$. Therefore, the Wiener index of the zigzag pentagon-based nanotubes, $I(p, 1)$ is as shown in Eq (3.3). □

Theorem 3.6. *When $p = 1$, the Wiener index of $I(1, q, \theta)$ is*

$$W(I(1,q,\theta)) = \begin{cases} 66, & q = 3; \\ \frac{9q^3}{8} + \frac{15q^2}{2} - \frac{101q}{8}, & q \geq 5 \text{ and } q \text{ is odd}; \\ \frac{9q^3}{8} + \frac{15q^2}{2} - \frac{25q}{2}, & q \geq 6 \text{ and } q \text{ is even}. \end{cases}$$

Proof. For $I(1, 3, \theta)$,

$$W(I(1,3)) = \frac{1}{2}\sum_{u\in V}\sum_{v\in V} d_{I(1,3)}(u,v) = 66.$$

For the Wiener index of the zigzag pentagon-based nanotubes $I(1, q, \theta)$, we analyze the cases where q is odd and even separately. As illustrated in Figure 28, when q is even, an a-left cut is applied to $I(1, q, \theta)$, partitioning the graph into two disjoint subgraphs $|A_1|$ and $|B_1|$. The graph $I(1, q, \theta)$ has a total of $3q$ vertices, where A_1 contains $3q - 5$ vertices and B_1 contains 5 vertices. At this time, $|A_1||B_1| = 5 \cdot (3q - 5)$. After removing the overlapping cuts, there are q left cuts starting from the boundary edge a-direction.

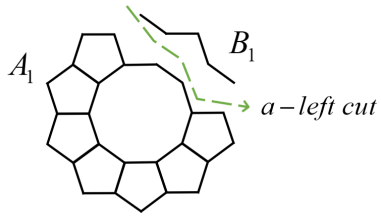

Figure 28. The a-left cut of $I(1, q, \theta)$.

As shown in Figure 29, in the case of even numbers, the a-right cut of $I(1, q, \theta)$ divides it into two parts, A_2 and B_2. The graph $I(1, q, \theta)$ contains a total of $3q$ vertices, and the A_2 part contains $\frac{3q}{2}$ vertices, while the B_2 part contains $\frac{3q}{2}$ vertices. At this time,

$$|A_2||B_2| = \frac{3q}{2} \cdot \frac{3q}{2}.$$

After removing the overlapping cuts, there are a total of q right cuts starting from the boundary edge a-direction.

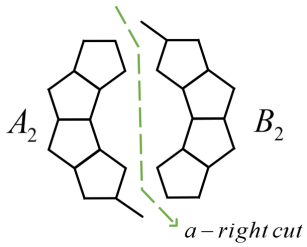

Figure 29. The a-right cut of $I(1, q, \theta)$.

For $q \geq 6$ and q is even,

$$\begin{aligned} W(I(1, q, \theta)) &= \frac{1}{2} \sum_{\{A,B\} \in C(G)} |A||B| \\ &= \frac{1}{2} \left[5 \cdot (3q - 5) \cdot q + \frac{3q}{2} \cdot \frac{3q}{2} \cdot q \right] \\ &= \frac{9q^3}{8} + \frac{15q^2}{2} - \frac{25q}{2}. \end{aligned}$$

As shown in Figure 30, in the case of odd numbers, the a-left cut of $I(1, q, \theta)$ divides it into two parts, A_3 and B_3. The graph $I(1, q, \theta)$ contains a total of $3q$ vertices, with A_3 containing $3q - 5$ vertices and B_3 containing 5 vertices. At this time,

$$|A_3||B_3| = 5 \cdot (3q - 5).$$

After removing the overlapping cuts, there are a total of q left cuts starting from the boundary edge a-direction.

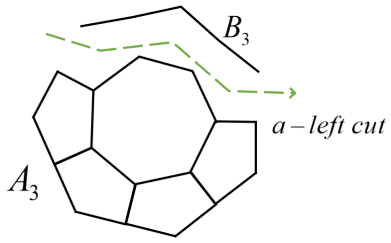

Figure 30. The a-left cut of $I(1, q, \theta)$.

As shown in Figure 31, in the case of odd numbers, the a-right cut of $I(1, q, \theta)$ divides it into two parts, A_4 and B_4. $I(1, q, \theta)$ contains a total of $3q$ vertices, with A_4 containing $\frac{3q+1}{2}$ vertices and B_4 containing $\frac{3q-1}{2}$ vertices. At this time,

$$|A_4||B_4| = \frac{3q+1}{2} \cdot \frac{3q-1}{2}.$$

After removing the overlapping cuts, there are a total of q right cuts starting from the boundary edge a-direction.

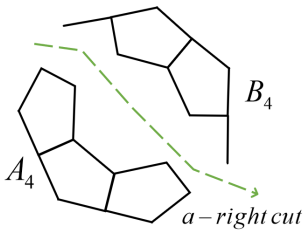

Figure 31. The a-right cut of $I(1, q, \theta)$.

For $q \geq 5$ and q is odd,

$$\begin{aligned} W(I(1, q, \theta)) &= \frac{1}{2} \sum_{\{A,B\} \in C(G)} |A||B| \\ &= \frac{1}{2}\left[5 \cdot (3q-5) \cdot q + \frac{3q+1}{2} \cdot \frac{3q-1}{2} \cdot q\right] \\ &= \frac{9q^3}{8} + \frac{15q^2}{2} - \frac{101q}{8}. \end{aligned}$$

□

Theorem 3.7. *The Wiener index of* $I(2, q, \zeta)$ *is*

$$W(I(2, q, \zeta)) = \begin{cases} 138, & q = 3; \\ 500, & q = 5. \end{cases}$$

Proof. For $I(2, 3, \zeta)$,

$$W(I(2, 3, \zeta)) = \frac{1}{2} \sum_{u \in V} \sum_{v \in V} d_{I(2,3)}(u, v) = 138.$$

For $I(2, 5, \zeta)$,

$$W(I(2, 5, \zeta)) = \frac{1}{2} \sum_{u \in V} \sum_{v \in V} d_{I(2,5)}(u, v) = 500.$$

□

3.3.2. The hyper-Wiener index of l_1-embeddable pentagon-based open-ended nanotubes

Theorem 3.8. *When $p = 1$, the hyper-Wiener index of $I(1, 3, \theta)$ is*

$$WW(I(1, 3, \theta)) = 204.$$

Proof. When $q = 3$, calculate the hyper-Wiener index of $I(1, 3, \theta)$ using the distance between pairs of vertices:

$$\begin{aligned} WW(I(1,3,\theta)) &= \frac{1}{2}\sum_{u\in V}\sum_{v\in V} d_{I(1,3,\theta)}(u,v) + \frac{1}{2}\sum_{u\in V}\sum_{v\in V} d_{I(1,3,\theta)}(u,v)^2 \\ &= 66 + \frac{1}{2}[(2*1+4*4+9*2)*3 + (3*1+4*4+9)*3 \\ &\quad + (3*1+4*4+9)*3] \\ &= 204. \end{aligned}$$

□

Theorem 3.9. *When $p = 2$, the hyper-Wiener index of $I(2, q, \zeta)$ is*

$$WW(I(2,q,\zeta)) = \begin{cases} 456, & q = 3; \\ 2040, & q = 5. \end{cases}$$

Proof. When $q = 3$, the hyper-Wiener index of $I(2, 3, \zeta)$ is computed using the distance between pairs of vertices:

$$\begin{aligned} WW(I(2,3,\zeta)) &= \frac{1}{2}\sum_{u\in V}\sum_{v\in V} d_{I(2,3,\zeta)}(u,v) + \frac{1}{2}\sum_{u\in V}\sum_{v\in V} d_{I(2,3,\zeta)}(u,v)^2 \\ &= 135 + \frac{1}{2}[(3*1+4*4+9*3+16*1)*3*2 \\ &\quad + (3*1+4*6+9*2)*3*2] \\ &= 456. \end{aligned}$$

When $q = 5$, the hyper-Wiener index of $I(2, 3, \zeta)$ is computed using the distance between pairs of vertices:

$$\begin{aligned} WW(I(2,5,\zeta)) &= \frac{1}{2}\sum_{u\in V}\sum_{v\in V} d_{I(2,5,\zeta)}(u,v) + \frac{1}{2}\sum_{u\in V}\sum_{v\in V} d_{I(2,5,\zeta)}(u,v)^2 \\ &= 500 + \frac{1}{2}(3*1+4*6+9*6+16*3+25*1)*3*4 \\ &= 2040. \end{aligned}$$

□

4. Conclusions

In this paper, we first discussed the l_1-embeddability of zigzag pentagon-based nanotubes by using convex cuts, 5-gonal inequality, and the edge labels. It can be concluded that only five types of zigzag pentagon-based nanotubes are l_1-graphs. It was found that all the armchair pentagon-based nanotubes

were not l_1-graphs. Based on the above research, we precisely obtained the Wiener index and the hyper-Wiener index of l_1-embeddable zigzag pentagon-based nanotubes. In the course of our next research, we will attempt to demonstrate the l_1-embeddability of pentagon-based nanotubes with irregular ends. In the pentagon-based nanotubes with irregular ends, it is extremely difficult to determine whether there are isometric subgraphs of $I(2, q, \zeta)$ within them. Therefore, the 5-gonal inequality cannot be used to determine its l_1-embeddability. Also, due to the uncertainty of the end shape, the directions of the cuts cannot be determined. All these have increased the difficulty of the research.

Author contributions

Guangfu Wang is responsible for the development of research frameworks, research tools and experimental paradigms, as well as the teaching, training and academic guidance for team members; Chunxiao Xu develops research methodologies and frameworks, and drafts original manuscript content for single or multiple sections of the article; Wenchao Cong adopts and appropriately revising esearch methods, and undertakes the review of figures, tables and supplementary materials for the research paper. All authors have read and agreed to the published version of the manuscript.

Use of Generative-AI tools declaration

The authors declare they have not used Artificial Intelligence (AI) tools in the creation of this article.

Acknowledgments

We would like to sincerely thank the Natural Science Foundation of Shandong Province (Grant No. ZR2024MA073) for funding this research.

Special thanks go to all reviewers for their precious remarks and constructive recommendations that have contributed significantly to the improvement of our manuscript.

Conflict of interest

All authors declare no conflicts of interest in this paper.

References

1. S. Zhang, J. Zhou, Q. Wang, X. Chen, Y. Kawazoe, P. Jena, Penta-graphene: a new carbon allotrope, *Proc. Natl. Acad. Sci. USA*, **112** (2015), 2372–2377. https://doi.org/10.1073/pnas.1416591112
2. C. Zhong, Y. Chen, Z. Yu, Y. Xie, H. Wang, S. A. Yang, et al. Three-dimensional pentagon carbon with a genesis of emergent fermions, *Nat. Commun.*, **8** (2017), 15641. https://doi.org/10.1038/ncomms15641
3. D. Liao, J. Zhang, S. Wang, Z. Zhang, A. Cortijo, M. A. H. Vozmediano, et al., Visualizing the topological pentagon states of a giant C_{540} metamaterial, *Nat. Commun.*, **15** (2024), 9644. https://doi.org/10.1038/s41467-024-53819-9

4. Y. Liu, L. Yuan, W. Chi, W. Han, J. Zhang, H. Pang, et al., Cairo pentagon tessellated covalent organic frameworks with mcm topology for near-infrared phototherapy, *Nat. Commun.*, **15** (2024), 7150. https://doi.org/10.1038/s41467-024-50761-8
5. A. Gupta, I. Newman, Y. Rabinovich, Alistair Sinclair, cuts, trees and l_1-embeddings of graphs, *Combinatorica*, **24** (2004), 233–269. https://doi.org/10.1007/s00493-004-0015-x
6. Y. Aumann, Y. Rabani, An $O(log\ k)$ approximate min-cut max-flow theorem and approximation algorithm, *SIAM J. Comput.*, **27** (1998), 291–301. https://doi.org/10.1137/S009753979428598
7. A. Blum, G. Konjevod, R. Ravi, S. Vempala, Semi-definite relaxations for minimum bandwidth and other vertex-ordering problems, *Theor. Comput. Sci.*, **235** (2000), 25–42. https://doi.org/10.1016/S0304-3975(99)00181-4
8. P. Assouad, M. Deza, Espaces métriques plongeables dans un hypercube: aspects combinatoires, *Ann. Discrete Math.*, **8** (1980), 197–210. https://doi.org/10.1016/S0167-5060(08)70874-4
9. S. Shpectorov, On scale embeddings of graphs into hypercubes, *Eur. J. Combin.*, **14** (1993), 117–130. https://doi.org/10.1006/eujc.1993.1016
10. V. Chepoi, M. Deza, V. Grishukhin, Clin d'oeil on l_1-embeddable planar graphs, *Discrete Appl. Math.*, **80** (1997), 3–19. https://doi.org/10.1016/S0166-218X(97)00066-8
11. D. Ž. Djoković, Distance-preserving subgraphs of hypercubes, *J. Combin. Theory Ser. B*, **14** (1973), 263–267. https://doi.org/10.1016/0095-8956(73)90010-5
12. I. Blake, J. Gilchrist, Addresses for graphs, *IEEE Trans. Inf. Theory*, **19** (1973), 683–688. https://doi.org/10.1109/TIT.1973.1055087
13. H. Zhang, G. Wang, Embeddability of open-ended carbon nanotubes in hypercubes, *Comput. Geom.*, **43** (2010), 524–534. https://doi.org/10.1016/j.comgeo.2009.12.001
14. G. Wang, C. Li, l_1-embeddability under the edge-gluing operation on some nonbipartite graphs, *Discrete Appl. Math.*, **375** (2025), 79–84. https://doi.org/10.1016/j.dam.2025.05.036
15. S. Klavžar, I. Gutman, B. Mohar, Labeling of benzenoid systems which reflects the vertex-distance relations, *J. Chem. Inf. Comput. Sci.*, **35** (1995), 590–593. https://doi.org/10.1021/ci00025a030
16. S. J. Cyvin, B. N. Cyvin, J. Brunvoll, E. Brendsdal, F. Zhang, X. Guo, et al., Theory of polypentagons, *J. Chem. Inf. Comput. Sci.*, **33** (1993), 466–474. https://doi.org/10.1021/ci00013a027
17. M. Deza, M. I. Shtogrin, Embeddings of chemical graphs in hypercubes, *Math. Notes*, **68** (2000), 295–305. https://doi.org/10.1007/BF02674552
18. H. Zhang, S. Xu, None of the coronoid systems can be isometrically embedded into a hypercube, *Discrete Appl. Math.*, **156** (2008), 2817–2822. https://doi.org/10.1016/j.dam.2007.11.010
19. A. Deza, M. Deza, V. Grishukhin, Fullerenes and coordination polyhedra versus half-cube embeddings, *Discrete Math.*, **192** (1998), 41–80. https://doi.org/10.1016/S0012-365X(98)00065-X
20. M. Marcušanu, *The classification of l_1-embeddable fullerenes*, Ph. D. thesis, Bowling Green State University, 2007.

21. M. Deza, P. W. Fowler, M. Shtogrin, Version of zones and zigzag structure in icosahedral fullerenes and icosadeltahedra, *J. Chem. Inf. Comput. Sci.*, **43** (2003), 595–599. https://doi.org/10.1021/ci0200669

22. H. Wiener, Structural determination of paraffin boiling points, *J. Amer. Chem. Soc.*, **69** (1947), 17–20. https://doi.org/10.1021/ja01193a005

23. H. Hosoya, Topological index: a newly proposed quantity characterizing the topological nature of structural isomers of saturated hydrocarbons, *Bull. Chem. Soc. Jpn.*, **44** (1971), 2332–2339. https://doi.org/10.1246/bcsj.44.2332

24. A. A. Dobrynin, R. Entringer, I. Gutman, Wiener index of trees: theory and applications, *Acta Appl. Math.*, **66** (2001), 211–249. https://doi.org/10.1023/A:1010767517079

25. B. Mohar, T. Pisanski, How to compute the Wiener index of a graph, *J. Math. Chem.*, **2** (1988), 267–277. https://doi.org/10.1007/BF01167206

26. V. Chepoi, S. Klavžar, The Wiener index and the szeged index of benzenoid systems in linear time, *J. Chem. Inf. Comput. Sci.*, **37** (1997), 752–755. https://doi.org/10.1021/ci9700079

27. M. Randić, Novel molecular descriptor for structure–property studies, *Chem. Phys. Lett.*, **211** (1993), 478–483. https://doi.org/10.1016/0009-2614(93)87094-J

28. D. J. Klein, I. Lukovits, I. Gutman, On the definition of the hyper-Wiener index for cycle-containing structures, *J. Chem. Inf. Comput. Sci.*, **35** (1995), 50–52. https://doi.org/10.1021/ci00023a007

29. K. Xu, M. Liu, I. Gutman, B. Furtula, A survey on graphs extremal with respect to distance-based topological indices, *Match Commun. Math. Comput. Chem.*, **71** (2014), 461–508.

30. I. Gutman, N. Trinajstić, Graph theory and molecular orbitals. Total φ-electron energy of alternant hydrocarbons, *Chem. Phys. Lett.*, **17** (1972), 535–538. https://doi.org/10.1016/0009-2614(72)85099-1

31. I. Gutman, B. Ruščić, N. Trinajstić, C. F. Wilcox, Graph theory and molecular orbitals. XII. Acyclic polyenes, *J. Chem. Phys.*, **62** (1975), 3399–3405. https://doi.org/10.1063/1.430994

32. H. Rahbani, H. A. Ahangar, M. A. Henning, New upper bounds on Zagreb indices with given domination number, *Appl. Math. Comput.*, **514** (2026), 129815. https://doi.org/10.1016/j.amc.2025.129815

33. G. Wang, Z. Xiong, L. Chen, l_1-embeddability of shifted quadrilateral cylinder graphs, *Graphs Combin.*, **39** (2023), 129. https://doi.org/10.1007/s00373-023-02725-w

34. G. Wang, Y. Liu, The edge-Wiener index of zigzag nanotubes, *Appl. Math. Comput.*, **377** (2020), 125191. https://doi.org/10.1016/j.amc.2020.125191

35. T. Ghosh, B. Mandal, Wiener indices of zigzag single walled carbon nanotubes and related nanotories, *Chem. Phys.*, **572** (2023), 111973. https://doi.org/10.1016/j.chemphys.2023.111973

36. G. Wang, Y. Liu, J. Wei, J. Liu, The edge-hyper-Wiener index of zigzag single-walled nanotubes, *Polyc. Aromat. Comp.*, **43** (2023), 1509–1523. https://doi.org/10.1080/10406638.2022.2030764

37. H. J. Bandelt, V. Chepoi, Decomposition and l_1-embedding of weakly median graphs, *Eur. J. Combin.*, **21** (2000), 701–714. https://doi.org/10.1006/eujc.1999.0377

38. M. Deza, V. Grishukhin, M. I. Shtogrin, *Scale-isometric polytopal graphs in hypercubes and cubic lattices: polytopes in hypercubes and Zn*, Imperial College Press, 2004. https://doi.org/10.1142/p308

39. G. Wang, H. Zhang, l_1-embeddability under the edge-gluing operation on graphs, *Discrete Math.*, **313** (2013), 2115–2118. https://doi.org/10.1016/j.disc.2013.04.032

40. M. E. Tylkin, On Hamming geometry of unitary cubes, *Dokl. Akad. Nauk SSSR*, **134** (1960), 1037–1040.

41. M. Deza, M. Laurent, *Geometry of cuts and metrics*, Springer, 1997. https://doi.org/10.1007/978-3-642-04295-9

42. J. H. Koolen, V. Moulton, D. Stevanović, The structure of spherical graphs, *Eur. J. Combin.*, **25** (2004), 299–310. https://doi.org/10.1016/S0195-6698(03)00116-1

43. V. Chepoi, On distances in benzenoid systems, *J. Chem. Inf. Comput. Sci.*, **36** (1996), 1169–1172. https://doi.org/10.1021/ci9600869

44. M. Deza, M. Laurent, l_1-rigid graphs, *J. Algebraic Combin.*, **3** (1994), 153–175. https://doi.org/10.1023/A:1022441506632

45. M. Deza, S. Shpectorov, Recognition of the l_1-graphs with complexity $O(nm)$, or football in a hypercube, *Eur. J. Combin.*, **17** (1996), 279–289. https://doi.org/10.1006/eujc.1996.0024

46. I. N. Cangul, A. Saleh, A. Alqesmah, H. Alashwali, Entire Wiener index of graphs, *Commun. Combin. Optim.*, **7** (2022), 227–245. https://doi.org/10.22049/CCO.2021.27234.1217

AIMS Press